BOLETIN DE LA SOCIEDAD ESPAÑOLA DE
Cerámica y Vidrio
www.elsevier.es/bsecv

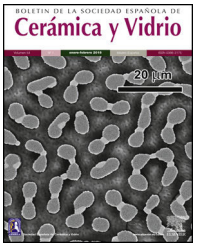

Synthesis and characterization of Faujasite-Na from fly ash by the fusion-hydrothermal method

Ricardo Adolfo Parra-Huertas, Carlos Ordulio Calderón-Carvajal, Jairo Alberto Gómez-Cuaspud, Enrique Vera-López*

Grupo de Integridad y Evaluación de Materiales (GIEM), Instituto para la Investigación e Innovación en Ciencia y Tecnología de Materiales (INCITEMA), Universidad Pedagógica y Tecnológica de Colombia, Av. Central del Norte 39-115, Tunja, Colombia

ARTICLE INFO

Article history:
Received 30 June 2022
Accepted 11 January 2023
Available online 4 February 2023

Keywords:
Aluminosilicates
Fly ash
Faujasite-Na
Fusion hydrothermal

ABSTRACT

This research focused on the synthesis and characterization of Faujasite-Na zeolites from fly ash (FA). The FA was subjected to pretreatment processes, washings with hydrochloric acid solutions and heat treatments at 700 °C for 3 h, to remove unburned carbon that would affect the synthetic process. After a fusion with NaOH at 550 °C for 3 h, the resulting material was disposed in a hydrothermal reactor at 100 °C for 12 h to obtain the corresponding zeolite. The products were characterized by XRD analysis, where quartz, mullite, sillimanite and lime phases were identified for the fly ash; quartz, mullite and in higher proportion Faujasite-Na for the synthesized material. The average size of the crystals of the fly ash and zeolite Faujasite-Na was 35.0 and 38.7 nm respectively, while the FTIR results allowed the identification of vibrational bands, characteristic of Si—O—Si and Si—O bonds. The TGA-DTA analysis, allowed the identification of signals associated with exothermic and endothermic processes related to water removal and Faujasite-Na formation, while the EDX analysis coupled to SEM allowed verifying that the composition of the samples is consistent with the results sought and that the morphological characteristics validate the proposed methodology. The XRF results confirm the composition of the fly ash and the obtained Faujasite in accordance with some previous results and an improved composition. Surface area analyses (BET) showed that synthesized Faujasite possess an active area of 460 $m^2\ g^{-1}$ while the fly ash for its physicochemical properties just an area of 6 $m^2\ g^{-1}$. The overall results confirmed the efficiency of Faujasite-Na synthesis from FA by the proposed fusion-hydrothermal method.

* *Corresponding author.*
E-mail address: ricardo.parra@uptc.edu.co (R.A. Parra-Huertas).
https://doi.org/10.1016/j.bsecv.2023.01.004

Síntesis y caracterización de Faujasita-Na a partir de ceniza volante por el método fusión hidrotermal

Palabras clave:
Aluminosilicatos
Ceniza volante
Faujasita-Na
Fusión-hidrotermal

R E S U M E N

Esta investigación se centró en la síntesis y caracterización de zeolitas Faujasita-Na a partir de cenizas volantes, las cuales fueron sometidas a procesos de pretratamiento, lavados con soluciones de ácido clorhídrico y tratamientos térmicos a 700 °C durante 3 h, para remover el carbón no quemado que afectaría el proceso de síntesis. Luego de una fusión con NaOH a 550 °C por 3 h, el material resultante se dispuso en un reactor hidrotermal a 100 °C durante 12 h para obtener la zeolita correspondiente. Los productos se caracterizaron mediante análisis de difracción de rayos X, donde se identificaron fases de cuarzo, mullita, silimanita y cal para las cenizas volantes; cuarzo, mullita y en mayor proporción Faujasita-Na para el material sintetizado. El tamaño medio de los cristales de las cenizas volantes y de la zeolita Faujasita-Na fue de 35,0 y 38,7 nm respectivamente, mientras los resultados de espectroscopia con infrarrojos permitieron la identificación de bandas vibracionales, características de los enlaces Si-O-Si y Si-O. El análisis TGA-DTA, permitió identificar señales asociadas a procesos exotérmicos y endotérmicos relacionados con la remoción de agua y formación de Faujasita-Na, mientras que el análisis EDX acoplado a SEM permitió verificar que la composición de las muestras es consistente con los resultados buscados y que las características morfológicas validan la metodología propuesta. Los resultados de XRF confirman la composición de las cenizas volantes y la Faujasita de acuerdo con algunos resultados anteriores y una composición mejorada. Los análisis de área superficial (BET) mostraron que la Faujasita sintetizada posee un área activa de 460,37 $m^2\ g^{-1}$ mientras que las cenizas volantes por sus propiedades fisicoquímicas solo tienen un área de 6 $m^2\ g^{-1}$. Los resultados generales confirmaron la eficiencia de la síntesis de Faujasita-Na a partir de cenizas volantes mediante el método hidrotermal de fusión propuesto.

Introduction

Coal is one of the most important fossil fuels for the development of the world economy, since 40% of the electrical energy generated today still depends on the combustion of this resource, which produces significant quantities of solid waste, one of the main by-products of which is the so-called fly ash (abbreviated FA) [1,3]. During combustion, each ton of pulverized coal burned generates approximately 200 kg of FA, so annual production worldwide is estimated at between 600 and 750 million tons [4,11]. In the case of Colombia, thermoelectric power plants, most of which are concentrated in the central region of Boyacá (Colombia), consuming around 61 tons h^{-1} of coal and produce approximately 8.1 tons h^{-1} of FA, of which the majority do not have the possibility of being reincorporated into production or value-added cycles to reduce its environmental impact [12].

Usually, most of the FA that can be collected and does not generate airborne particulate pollutants is disposed in landfills, occupying land that could be used for other purposes and causing fundamental environmental problems [2]. Thus, among the various research efforts that have been made to efficiently process this type of waste and convert them into products that can be reincorporated into value-added production cycles, is the use of these materials as raw materials in obtaining synthetic zeolites. These have wide applicability in fields such as agriculture, medicine, industry and environmental engineering as optimal systems for the storage and transport of chemical species, wastewater treatment through the possibility of capturing heavy metals and others as intermediaries in obtaining other compounds of higher added value [3].

In accordance with [13,14], these FA could be utilized as building materials, construction of roads and in the agriculture; however, the utilization rate is less than 47%, and the added value of utilization is low [15]. In some cases, such utilization rate propitiate that large quantities of stored fly ash seriously destroy the ecological environment and occupy some land resources [14,16], causing serious air and water pollution and increase in the human desease risks [14,15].

Usually, the fly ash is rich in Si and Al oxides, which are the most common starting reagents for production of zeolites [15], offering an excellent opportunity for cost reduction and mitigation of environmental impacts [17], being the Class F silica type, one of the most characteristic for zeolite production due to its rich alumina-silica content with some minerals that contain quartz, mullite minerals and aluminosilicates glassy phases in a lot of probable application fields [15,18].

Although most zeolites are hydrated aluminosilicates with a microporous crystal structure of tetrahedral SiO_4 and AlO_4 units interconnected by oxygen atoms [19,20], not all of these have the same characteristics [21,22]. Among others the Faujasite-Na (abbreviated FAU) is one of the most attractive systems, since it has a three-dimensional porous channel structure, consisting of interconnected six-membered double

ring cages with an octahedral morphology and cubic crystal structure [23–25]. Due to its negatively charged surface, the internal pores, the chemical composition and the particular size of structure [19–26], this material represents one of the most relevant zeolites for use in various industrial applications such as catalysis, adsorption, ion exchange [25–27], catalytic cracking, adsorption of volatile organic compounds, adsorption for air dehumidification and adsorptive separation of $O_{2(g)}$ and $N_{2(g)}$ between others [25,28].

Considering the relevance of FAU zeolites and the large amount of FA derived from energy production processes in the region of Boyacá-Colombia, that can be reused and recycled into a circular economy model, the objective of this research is oriented toward obtention of FAU type zeolite by hydrothermal fusion reaction, in order to evaluate the effectiveness of the proposed method through the qualitative and quantitative characterization of the final product with respect to the starting material used.

Materials and methods

Preliminary treatment of fly ash

The FA used was initially grounded in a PM-400 RETSCH planetary mill until a fine powder was obtained, which was then sieved at 100 μm mesh [29], in order to generate a homogeneous material for the subsequent stages of the method. The pulverized material was subjected to ultrasonic treatment in a BRANSON 1800 equipment for 1 hour at 50 °C and 40 kHz to remove some unburned residues [28]. Subsequently, the collected material was dried at 90 °C for 24 h from the previous step and was treated with 3.0 mol L^{-1} hydrochloric acid solutions to remove impurities such as Fe_2O_3, using a weight ratio of 1:2 at a temperature of 60 °C for 1.5 h completing five washing cycles as indicated in previous references [11,30]. At the end of the acid treatment processes, the solid was washed with double distilled water until pH values between 6 and 7 were reached to ensure that the residual acid had been removed [27,31].

The collected ash was again dried at 90 °C for 24 h and subsequently taken to calcination at 700 °C in a TERRIGENO FPCA muffle furnace for 3 h at a heating rate of 1 °C min^{-1} to remove carbonaceous residues [2].

Hydrothermal treatment

Hydrothermal synthesis method is the earliest and most commonly used method for synthesizing zeolite, which has occupied an important position so far [32], using temperature ranges of synthesis from 100 to 240 °C. The advantages of the HT synthesis are that products have high purity, in general represents a low energy consumption and low environmental impact since the reaction proceed under a controlled atmosphere [32]. For this reason is one of the most widely employed methods for the production of zeolite starting from alkaline solutions [33].

Typically, under the commonly used synthesis process, a sealed vessel usually made of polypropylene or Teflon is used in a steel autoclave, requiring a lower synthesis temperature in comparison to other methods [34], the samples of FA are treated with sodium hydroxide (NaOH) are fused at 550 °C prior to conventional raised temperature treatment without stirring. In this work, a novel approach enabled to produce synthetic zeolite with a high conversion rate and improved crystallinity according to previous works [33].

The literature commonly recommends a pre-fusion step improves the traditionally used hydrothermal treatment that has been confirmed with numerous studies. The major disadvantage could be raised temperature treatment (500–600 °C) that adds up to the costs of the method [33]. Although, the hydrothermal technique is considered as a primary route of the synthesis of zeolites [21], these are habitually synthesized via alkaline fusion followed by hydrothermal treatment from fly ash approach in two reaction stages [21,32,35,37], which, includes low energy consumption, the high re-activity, lower air pollution, formation of metastable phases and unique condensed phases [34].

Conventionally, the alkaline fusion-assisted hydrothermal method was introduced to improve the yield and quality of the zeolite synthesis by means the mixture of FA and alkali at a high temperature and a processing of a melt product is processed through hydrothermal treatment [21]. For the proper treatment of fly ash, the alkaline fusion-hydrothermal method involves mixing alkaline substances (Na_2CO_3, NaOH, etc.) in a certain proportion, which treated in a muffle furnace, promotes the effectively reaction of the glassy structure of the fly ash by high temperature. Then, under the combined action of an alkali activator, the original structure of inert components in fly ash (such as quartz stone and mullite ($3Al_2O_3{\cdot}2SiO_2$), collapse to release silicon and aluminum elements. After the alkaline fusion, the surface of the fly ash contains a large amount of amorphous silicon and aluminum elements that can be used to improve the synthesis rate and quality of zeolite through the subsequent hydrothermal reaction [38].

Previous works, also have founded that mullite can be fully hydrolyzed and converted into zeolite by adding a small amount of water to the mixture of FA and NaOH before melting and that a low NaOH concentration leads to a small extraction amount of aluminum silicate in FA, which is not appropriate to the formation of zeolite. However, excessive NaOH enrichment results in the conversion of zeolite to hydroxysodalite. Zeolites synthesized through the alkali fusion method, have a higher specific surface area, cation exchange capacity, and crystallinity than those synthesized using the traditional hydrothermal method [21], which involves at least one liquid phase and one solid amorphous phase that could be affected by aspects as the temperature, the reaction time and the pressure [38].

Zeolite synthesis

The synthesis process comprised two stages, alkaline fusion and hydrothermal reaction according to the reported methodology by Feng et al. [2]. In the alkaline fusion process, the FA was mixed with sodium hydroxide powder in a 1:1.2 ratio by weight to obtain a homogeneous mixture. In the second instance, the above mixture was heat treated in a platinum crucible at 550 °C for 3 h in a muffle-type furnace [39] and the resulting solid was mixed with distilled water at a ratio of

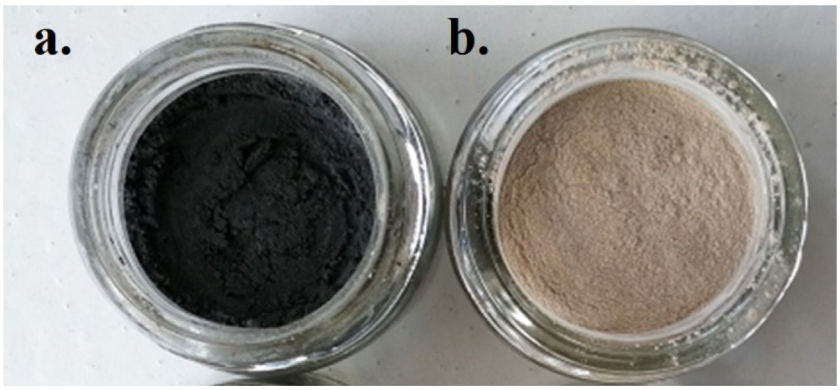

Fig. 1 – (a) FA without treatment and (b) after ultrasonic washing with 3.0 mol L^{-1} HCl.

4.89 mL per gram of FA under magnetic stirring conditions for 24 h [40]. The resulting mixture was arranged for hydrothermal treatment in a stainless-steel reactor with Teflon internal coating at a temperature of 100 °C in an MEMMERT UN55 oven for 12 h [40]. Finally, the synthesized solid was recovered by vacuum filtration and dried at 105 °C for 24 h in a convection oven [41].

Characterization of the fly ash and zeolite synthesized

The FA and synthesized FAU were characterized by X-ray diffraction (XRD), infrared spectroscopy (FTIR), thermogravimetric analyses (TGA), differential thermal analysis (DTA), morphological (SEM) and compositional analysis by scanning electron microscopy coupled to X-ray dispersive analysis (EDX).

The structural characterization by X-ray diffraction technique was performed in an X'pert PANanalitical PRO-MPD equipment, equipped with an Ultrafast X'Celerator detector in Bragg-Brentano configuration using Cu Kα radiation (λ = 1.54 Å) between 10 and 90° with steps of 0.02° with a voltage of 40 kV. The diffraction patterns obtained were indexed and analyzed in the X'Pert HighScore Plus software [42] and refined by the Rietveld method in the GSAS software [43], using the crystallographic information files (.cif) [44] of the American Mineralogist Crystal Database (AMCSD) for the phases coincident with the data obtained in the experiment [45]. The average size of the crystals was calculated by means of the Debye Scherrer equation:

$$D = \frac{K\lambda}{\beta \cos \theta}$$

where K is the Scherrer constant, λ is wavelength of the X-ray beam used (1.54 Å), β is the Full width at half maximum (FWHM) of the peak and θ is the Bragg angle. The K constant is related with the shape of the particle being the most used a standard value of 0.89, which describes the broadening of some signals due to crystallite size [1]. The crystal size calculation was performed using the X'Pert HighScore tool called Scherrer calculator [2].

Infrared spectroscopy (FTIR) analyses were performed between 4700–500 cm^{-1} in a Shimadzu IRSpirit-T with a deuterium lamp and neon laser source in ATR configuration. The thermogravimetric analyses were performed on a NETZSCH-Gerätebau GmbH STA 2500 Regulus Simultaneous TGA-DTA Thermal Analyzer with a resolution of 0.03 g, using in all cases a sample weight of 200 mg and an air flow of 5 mL min^{-1}. In each case, the samples were analyzed after purge processes at 1050 °C using argon gas purge flow rate of 20 mL min^{-1} during 20 min.

The morphological and compositional aspects were determined by scanning electron microscopy (SEM-EDX) in a RA-Zeiss-001 EVO-MA10 equipment furnished with Oxford X-ray dispersive spectrometry. In all cases, the distance between the electron gun and the sample was kept at 8.5 mm (WD). The applied energy was 20 kV and a secondary electron detector was used. The materials were prepared in an aluminum sample holder, using adhesive carbon disks and the samples coated with gold to reduce the static charge and improve the quality of the images.

The chemical composition were further analyzed by X-ray fluorescence (PANAlytical MiniPal PW4025) using a helium atmosphere, the X-ray tube was made of rhodium with a voltage of 13 kV and a current of 0.012 mA.

For the specific surface area and pore size distribution, nitrogen sorption/desorption measurements were carried out with a Micromeritics instrument ASAP 2020. Prior to the analysis, the samples were submitted to a cleaning step for 6 h in a vacuum a 150 °C. Mathematic models were employed using Brunauer–Emmett–Teller (BET) and Barrett–Joyner–Halenda (BJH) models to determine the surface area and pore data.

Results and discussion

Fly ash

Fig. 1 shows the different stages of the change in physical appearance of the FA after the different processes, initially developed to avoid the presence of unburned and iron oxide impurities. The diffraction patterns shown in Fig. 2 corresponding to FA structure reveal that this starting material has crystalline structures in its composition, which agree with the AMCSD indexed patterns 0001059, 0011007, 0004110, 0008315 and 0000128, consistent with mullite (M), quartz (Q), sillimanite (S) and lime (L) phases.

Indexing of the main signals in the pattern corresponding to FA revealed the corresponding phases of mullite, quartz

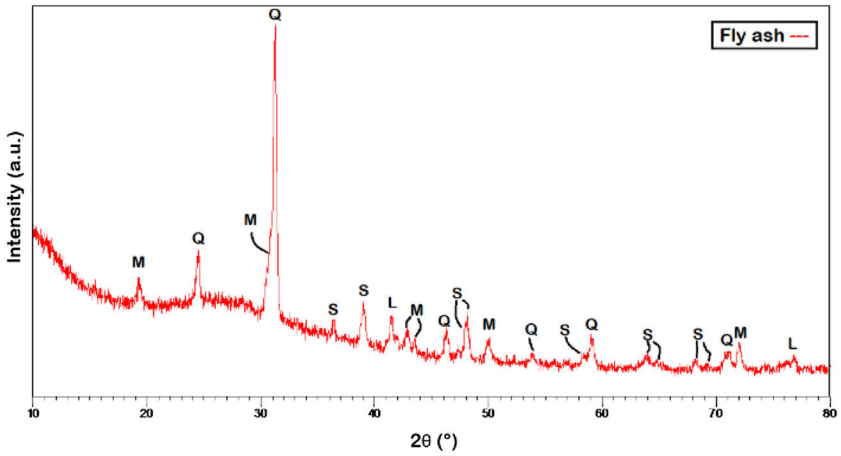

Fig. 2 – X-ray diffraction pattern for the FA sample identifying the phases of M: mullite, Q: quartz, S: sillimanite and L: lime.

and sillimanite, found the most intense signals around 30.05°, 31.45° and 39.04° 2θ respectively as indicated in preliminary cases [2,3,12,30,34,35]. The identification of such structures distributed along the diffraction pattern was based on the signals located above 41.80° and 77.20° 2θ for the case of the lime phase, in agreement with Li et al. [46].

From these results is clear that at high temperatures, NaOH act as mineralizing agent dissolving a large amount of silicon and aluminum of FA and according to Kunecki et al. [41] permit the obtention of mullite and quartz phases using a dissolution of NaOH 3.0 M at 80 °C, with reaction times of 24 h.

For Amoni et al. [47], in the hydrothermal synthesis route, the identification of the quartz, mullite, hematite and magnetite phases is very common, with nucleation processes that occurs rapidly on the surface of particles and forms a unique crystal structure [48] which composition depends of the corresponding fly ash origin. For other authors [18,49,50] the samples after synthesis could be composed mainly quartz, mullite, hematite, magnetite and limestone phases, being the Faujasite a compound which could be improved by the use of a via alkaline fusion followed by the addition of destilled water according to Joseph et al. [37] and Gjyli et al. [51].

Table 1 shows the structural details (crystalline system, space group, and cell constants) of the phases used to perform the quantitative analysis by the Rietveld method of the obtained diffraction pattern. Comparing the lattice parameters of Tables 1 and 2 obtained from the structural refinement of fly ash and zeolite with respect to those reported in the crystallographic information file (CIF) for a fused commercial mullite reported by Ross and Prewitt [52], it is found that they agree, therefore the same space group (*Pbam*) and similar cell volume are obtained, crystallizing in the orthorhombic system. In the case of quartz, the CIF values reported by Glinnemann et al. [53] are similar for this compound which was subjected to high pressures in their investigation, presenting the same space group ($P3_121$) and similar cell volume in the trigonal system. The sillimanite in the fly ash compared with the CIF values identified by Burt et al. [54] presented similar values of cell volume and space group *Pbnm*.

Fig. 3 shows the refined structure of FA where the adjustment of the signals with the experimental data is evidenced,

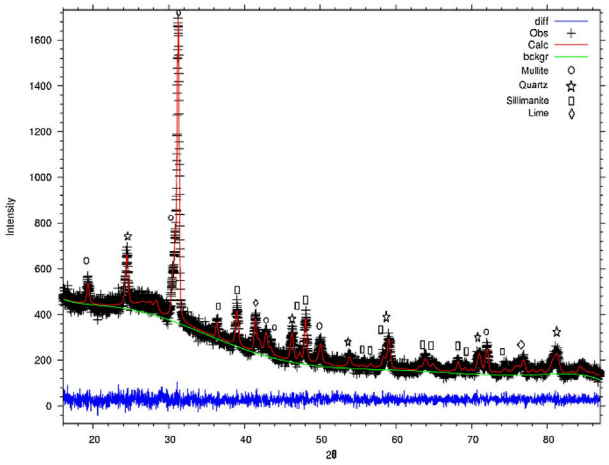

Fig. 3 – Rietveld refinement analysis of the FA sample.

obtaining a calculated pattern similar to the experimental data. From the refinement it was possible to define the weight percentage of each phase in the FA. Table 3 describes the quantitative analysis of the majority phases of mullite ($Al_6Si_2O_{13}$), quartz (SiO_2) with fragments of FA, mainly composed of sillimanite (Al_2SiO_5) 4.88% and lime (CaO) in 3.03% and being the phase that contributes to necessary Ca quantity to form the Faujasite-Na structure during the synthesis processes of these zeolites [46]. Table 4 describes the quantitative analysis of the majority phases of mullite ($Al_6Si_2O_{13}$), quartz (SiO_2) and Faujasite-Na $(Si_{4.2}Al_{1.8})Na_{0.15}\ Ca_{0.075}O_{13.333}H_{1.333}$.

Tables 3 and 4 also show the residual values obtained after crystallographic phase refinement, which indicate the quality of the refinement: $R_{wp} = 1.36\%$, $R_p = 2.67\%$ and the degree of fit (χ^2) which was 0.80, converging satisfactorily as shown in Fig. 3 [55].

Fig. 4 shows the infrared spectrum corresponding to FA with its main vibrational bands, as detailed in Table 5. The results are in agreement with the work of Abdelrahman [56] and Somderam et al. [57] regarding the vibrational bands responsible for the asymmetric T—O—T stretching signals

Table 1 – Structural parameters for the coincident phases identified by XRD for fly ash sample.

Phase	α	β	γ	a (Å)	b (Å)	c (Å)
Mullite	90	90	90	7.5785	7.6817	2.8864
Quartz	90	90	120	4.9210	4.9210	5.4163
Sillimanite	90	90	90	7.4604	7.6395	5.7584
Lime	90	90	90	4.9070	4.9070	4.9070

Phase	Cell volume (Å^3)	Crystalline system	Space group	Code AMCSD
Mullite	168.0340	Orthorhombic	*Pbam*	0001059
Quartz	113.5900	Trigonal	$P3_121$	0011007
Sillimanite	296.1190	Hexagonal	*Pbnm*	0004110
Lime	118.1540	Cubic	*Fm3m*	0008315

Table 2 – Structural parameters for the matched phases identified by XRD for the synthesized zeolite.

Phase	α	β	γ	a (Å)	b (Å)	c (Å)
Mullite	90	90	90	7.57	7.68	2.88
Quartz	90	90	120	4.92	4.92	5.41
Faujasite-Na	90	90	90	24.74	24.74	24.70

Phase	Cell volume (Å^3)	Crystalline system	Space group	Code AMCSD
Mullite	168.03	Orthorhombic	*Pbam*	000105
Quartz	113.59	Trigonal	$P3_121$	001100
Faujasite-Na	15,142.55	Cubic	*Pd3m*	000012

Table 3 – Comparison of FA quantification by Rietveld method in GSAS and FullProf software.

Phase	Chemical composition	Wt % estimated by GSAS	Wt % estimated by FullProf	Code AMCSD
Mullite	$Al_{2.38}\ Si_{0.62}\ O_{4.77}$	30.51	31.85	0001059
Quartz	SiO_2	61.58	62.14	0011007
Sillimanite	Al_2SiO_5	4.88	3.49	0004110
Lime	CaO	3.03	2.52	0008315
Refining parameters (GSAS)	$R_p = 2.67$	$R_{wp} = 1.36$	$\chi^{22} = 0.80$	
Refining parameters (FullProf)	$R_p = 2.92$	$R_{wp} = 1.71$	$\chi^{22} = 0.88$	

Table 4 – Refinement data by the Rietveld method for the diffractograms of the synthesized zeolite.

Phase	Chemical formula	Wt% in zeolite	Code AMCSD
Mullite	$Al_{2.38}\ Si_{0.62}\ O_{4.77}$	24.82	0001059
Quartz	SiO_2	12.90	0011007
Faujasite-Na	$(Si_{4.2}Al_{1.8})Na_{0.15}Ca_{0.075}O_{13.333}H_{1.333}$	62.28	0000128
Refining parameters	$R_p = 12.32$	$R_{wp} = 6.24$	χ^2 Y= 1.20

Table 5 – Transmittance signals for FA and synthesized FAU zeolite with its respective infrared active wavelength.

Band number	Wavelength (cm^{-1})	Type of bond
1	667	T—O—T (T = Si, Al)
2	748	Si—O—Si
3	1058	Si—O—Al
4	2854–2924	CH_4
5	660	T—O—T (T = Si, Al)
6	748	Si—O—Si
7	955	Al—O y Si—O
8	1651	H—O—H (Vibration bending)
9	2854–2924	CH_4
10	3450–3750	Si—OH, —OH

(T = Si, Al), attributed to the main oxidic structures of this type of materials.

The bands located above 545 and 748 cm^{-1} are related to the symmetric and asymmetric modes of vibration of the tetrahedron formed by the Si—O—Si bonds [58], while the band located at 1058 cm^{-1} is attributed to the antisymmetric stretching mode of vibration corresponding to the Si—O—Al bonds, as previously identified [59,60]. These signals are characteristic of semi-crystalline amorphous of varied compositions and related to aluminosilicates as the main components of FA, which are generally evidenced by the oxygen bonds with different aluminum and silicon tetrahedral forming structures of different number of members [60].

Although it is true that all the analyzed signals agree with the chemical profile of these raw materials, it is clear that the inverse signal located above 2854 cm^{-1} and 2924 cm^{-1} was associated with the presence of unburned products that

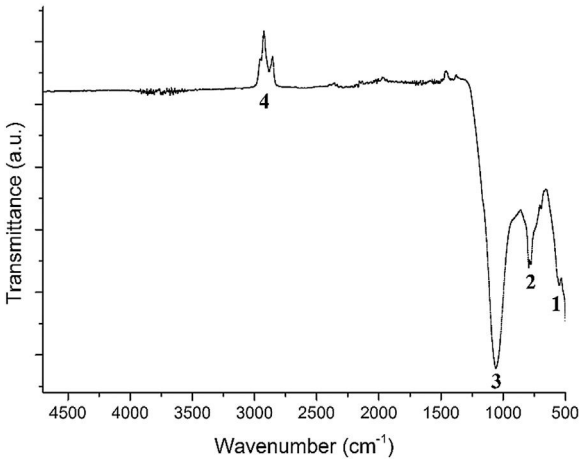

Fig. 4 – Infrared spectrum of the FA sample with its main vibrational bands.

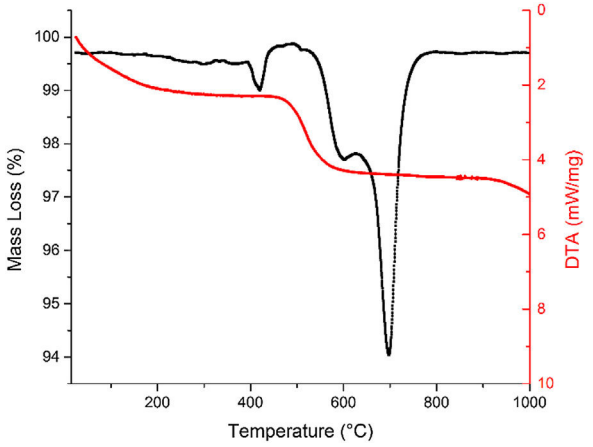

Fig. 5 – Thermal analysis of FA performed between room temperature and 1000 °C.

are not completely eliminated in the coal combustion processes and preliminary treatments. These signals are formed by vibrational bonds attributed to the C—H bond as has been previously reported and whose results are consistent with the methodology developed in this work to eliminate this type of impurities in the raw material to obtain zeolites [61].

Fig. 5 shows the results of the thermal analysis performed on the FA sample, where it can be observed that there is no significant variation in the TGA curve in relation to temperature. The curve stabilizes with overall losses of 2.5% mass up to a temperature of 1000 °C, which shows that the starting material has a relatively low surface humidity and unburned content. The changes initially recorded up to 400 °C, show mass losses of about 0.5% which is attributed to humidity loss, decomposition of some organic species and dehydroxylation phenomena of some aluminosilicates, which can be verified by the presence of an endothermic signal around 403.6 °C.

In Fig. 5, two additional signals located at 600.5 °C and 702.8 °C attributed to the quartz and mullite phases respectively, are consistent with the works of Tironi et al. and Valášková et al. [62,63], according to which some endothermic signals with values of approximately 4.0 mW mg^{-1} can be attributed to the effect of the CaO/SiO ratio of FA on the phase transitions, according to which some residuals as $CaCO_3$ and iron oxides trapped in the pores of these materials affect the DTA curve. Finally, it is evident that the sample evolves to a transition that relates to mullite with values of 9.2 mW mg^{-1} above 702.8 °C in accordance with [63].

The elemental composition of the FA was determined using the energy dispersive X-ray analysis (SEM-EDX), being consistent with the results found by structural characterization as shown in Fig. 6 and images of irregular solids as shown in Fig. 7. The elemental composition determined by EDX corresponds with the structural phases identified by diffraction analysis, where the FA is composed of C, Si, Al, O and Ca in 1.75, 32.20, 13.44, 50.54 and 2.07% respectively, elements necessary for the synthesis of zeolite-type materials. In this regard Iqbal et al. [9], reports percentage values of Si, Al and Ca of 11.18, 5.14 and 19.47% respectively in the FA consistent with the composition of the raw material proposed in the current work.

Studies carried out by scanning electron microscopy, reveal that the particles that constituted the FA have a predominantly spherical morphology with several characteristics (microspheres, spheres and plerospheres) [41,64,11] and to a

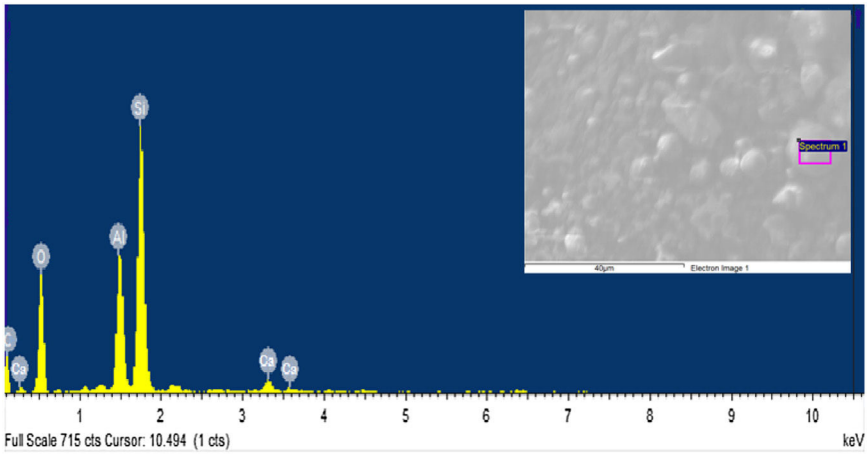

Fig. 6 – EDX-type analysis of the FA sample used as a precursor for Faujasite-Na sample.

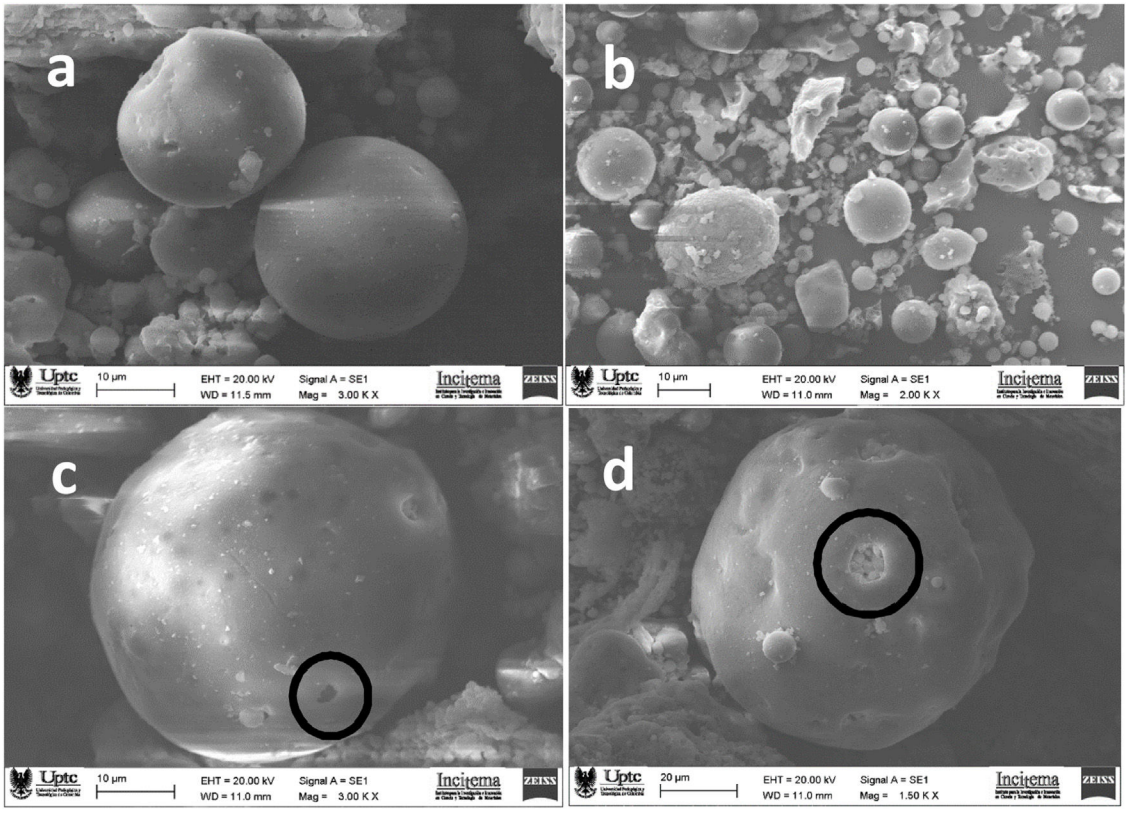

Fig. 7 – Scanning electron microscopy images for FA obtained at different magnifications.

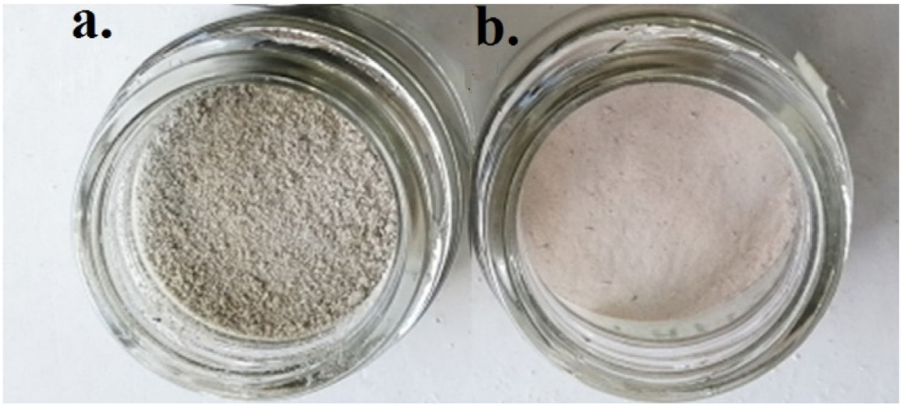

Fig. 8 – (a) FA after fusion with NaOH. (b) Synthesized FAU zeolite.

relatively smooth surface [48] of glassy aluminosilicate, which has been fully identified [37].

According to Ju et al. [14] the morphological characteristics of FA composed by amorphous silica, is related to a relatively smooth surface, which do not change after calcination, where there no apparent micropores and holes on the surface, which is consistent with the results obtained from N_2 adsorption–desorption isotherms [65]. These morphologic structures correspond to mullite, quartz and hematite [41], in accordance with the XRD results, where is clear that the amorphous coal fly ash are mainly composed by globular glass beads with different sizes, formed during the coal treatment at high temperatures in the gasification process as has been reported by Zhang et al. [31] and the SEM images shown in Fig. 7.

The micrographs in Fig. 7a and b reveal that the FA particles correspond with a spherical shape associated with amorphous aluminosilicate glassy material of submicrometer size [14,41]. According to the work of Feng et al. [2] and Yoldi et al. [19] this spherical shape is the result of sudden cooling processes during the coal combustion process in the formation of FA [66,67]. Fig. 7c and d shows hollow spheres known as cenospheres which are the result of the expansion of CO_2 gas and water vapor, when coal is burning and may contain smaller particles inside them called regular-appearing plerospheres [4,9–14,64–66].

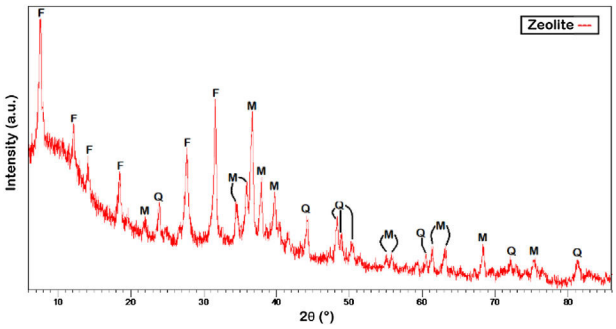

Fig. 9 – X-ray diffraction pattern for the FAU zeolite sample obtained, indicating the presence of F: Faujasite-Na, M: mullite and Q: quartz phases mainly.

Faujasite-Na

Fig. 8a shows the change in appearance of the FA after fusion with NaOH, where the formation of a new substance with high humidity content is observed. The material shown in Fig. 8b, of homogeneous appearance, white in color and with a different texture from initial conditions, permit to identify a chemical change due to evolution of FA to FAU material. The structural characterization of the obtained material after the proposed synthesis processes, indicates the formation of a new structure as a result of the treatments performed on the starting material consistent with a Faujasite-Na (F) type zeolite, as shown in Fig. 9.

According to Yang et al. [1] in the alkaline-hydrothermal synthesis, the activators convert SiO_2 and Al_2O_3 into zeolite crystalline phases weakening the chemical binding between SiO_2 and Al_2O_3 in the α-quartz and mullite crystal phases of fly ash, producing a large number of defects that cause particle movement inducing a thermodynamically unstable state, and forming soluble amorphous Si and Al [1] that not help to Faujasite-Na zeolite production. About this, has been found that Na^+ ions, are an activator with a good promotion effect on the nucleation and crystallization of the zeolite synthesis process, which is consistent with XRD measurements [36], since stabilize the sub-building of units and are fundamental in the enhance the product crystallinity [14,36]. Thus a low amount of NaOH is not effective to convert fly ash to soluble silicate and aluminate salts as well as resulting in no zeolite due to low crystallization rate. In contrast, a high amount of NaOH produces more stable zeolites like in current research [36].

With respect to the FA/NaOH relation mass ratio from 1:1.2 result that a slightly increase of crystallinity, produce an effective way to convert the FA into soluble silicates and aluminate salts, resulting in zeolites of high crystallization rate in consistence with works of Taunavov et al. [33]. Some studies developed by Zhang et al. [68], using a superior FA/NaOH relation mass ratio to 1:1.2 by alkaline fusion-hydrothermal method, permit the obtention of Faujasite zeolite with high intensity in XRD patterns, such results are supported by the works of Ren et al. [27], and Sivalingam et al. [30].

The indexing of the signals revealed the presence of Faujasite-Na, mullite and quartz, where most of the diffraction signals become evident around 8.05°, 12.05°, 14.10°, 18.50°, 28.00° and 32.50° 2θ respectively, in agreement with preliminary works [28]. Fig. 10 shows the unit cell corresponding to the FAU structure plotted in the VESTA software [69] from the corresponding CIF file with code AMCSD 0000128.

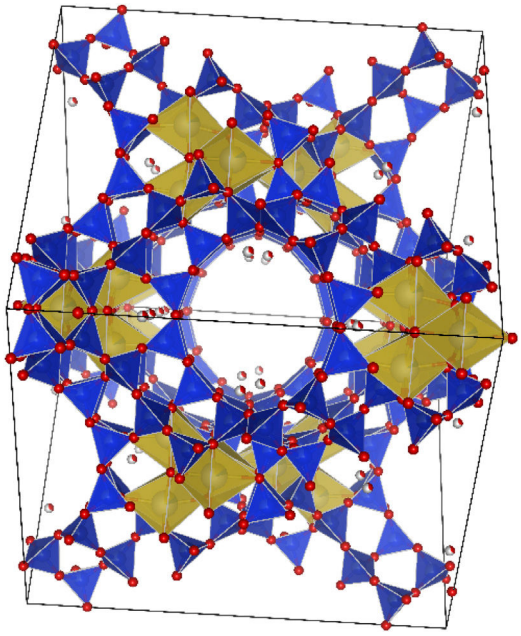

Fig. 10 – Unit cell of the Faujasite-Na type zeolite structure obtained from X-ray diffraction data.

X-ray diffraction patterns show distinct crystalline features predominantly composed of Faujasite type zeolite, where is evident that the main zeolite signals, are due to the traces of undissolved quartz and mullite during the reaction [15,32]. A fusion step before hydrothermal treatment of the FA produce different kind of zeolites, improving the dissolution of Si and Al content from parent FA, hence enhancing the yield of synthesis [33].

Essentially, the fusion of the NaOH and fly ashes facilitates the formation of highly active Na-silicates and Na-aluminates, which are readily dissolvable in aqueous solution and enhance zeolite formation significantly. The concentration of aluminosilicates, Na-silicates and Na-aluminates in the reaction system can precipitate zeolites more easily [65], reason why the alkalinity level has been indicated as a decisive factor on the nucleation of water-soluble minerals, the crystallization and the dissolution of the fusion products in accordance with Akin et al., 2021 [18].

The results in Fig. 9 indicated that the hydrothermal temperature had an evident effect on the phases concentration of the products; however, the diffraction signals associated to quartz and mullite indicate that coal fly ash was not completely dissolved under current reaction conditions and constituting a improve factor for next works.

The average size of the crystals of the fly ash and zeolite Faujasite-Na was 35.0 and 38.7 nm, respectively. The values for the crystallite size of the synthesized Faujasite-Na closely approximate those calculated with the Debye Scherrer equation reported by Abdelrahman [59] and Reinoso et al. [28]. In this regard, Sivalingam et al. [30] reported crystal sizes around

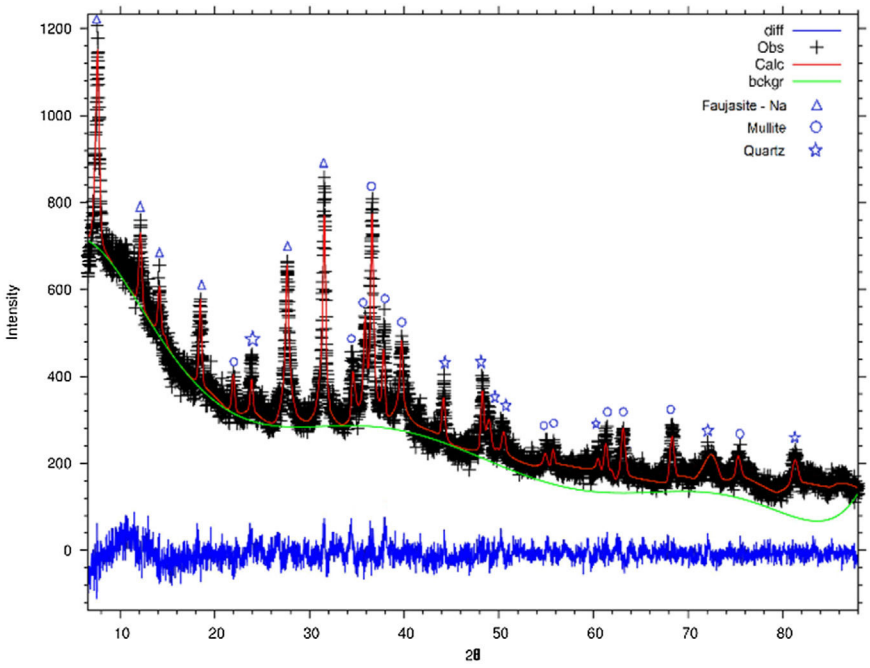

Fig. 11 – Rietveld refinement analysis of the synthesized FAU zeolite sample.

of 28.71–35.73 nm for Faujasite zeolite, while Reinoso et al. [28] reported under similar reaction conditions crystal sizes of 38–45 nm for Faujasite-Na. In the work of Abdelrahman et al. [59], the average crystallite size for obtained Faujasite was 39.09 nm, which reveal the effectiveness of current work.

The valuation of primary crystal size estimated from Scherrer equation corresponds with very small crystals smaller than 45 nm, aspect related to incorporation of ultrasound treatment at the aging stage, which decreases the crystallite size in accordance with Reinoso et al. [28] and the corresponding increase of the crystallite size during hydrothermal treatment.

Table 2 shows the structural details (crystalline system, space group, and cell constants) of the phases used to perform the quantitative analysis by the Rietveld method using the diffraction pattern of the synthesized material. For the faujasite, the value reported by CIF in the work of Baur et al. [70], reported a hexagonal group for a faujasite of natural origin.

Fig. 11 shows the refined pattern of the synthesized material where the fit of the phase signals with the experimental data is evident. From the refinement it was possible to determine the weight percentage of each phase in the synthesized material. According to Table 4, the majority phase in the synthesized material is according with the Faujasite-Na zeolite ($(Si_{4.2}Al_{1.8})Na_{0.15}Ca_{0.075}O_{13.333}H_{1.333}$) with a quantitative percentage of 62.28%, whereas mullite ($Al_6Si_2O_{13}$) and the quartz (SiO_2) are present in a minority with 24.82 and 12.90%, respectively, in agreement with Li et al. [46].

Table 4 also shows the residual values obtained after crystallographic phase refinement, which indicate the quality of the refinement: $R_{wp} = 6.24\%$, $R_p = 12.32\%$ and the degree of fit (χ^2) which was 1.20, indicating that the fit converged satisfactorily as shown in Fig. 11 [55].

Fig. 12 shows the infrared spectrum corresponding to the synthesized sample of FAU, as shown in Table 5, the bands

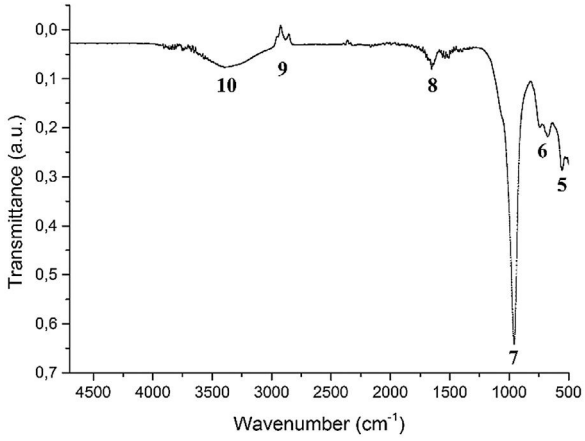

Fig. 12 – Infrared spectrum of the Faujasite-Na sample with its main vibrational modes.

located in the region of 500–660 cm^{-1} were associated with the vibrations of the double rings, specifically the band at 555 cm^{-1} is due to secondary structures D6R characteristic of the Faujasite-Na [1–8,37–40,53], in addition to asymmetric and symmetric stretching-type vibrations of T—O bonds (T = Si, Al) [71]. The 748 cm^{-1} band is related to asymmetric and symmetric vibrational modes of a tetrahedron, attributed to internal vibrations in the Si—O—Si bonds [58].

The 955 cm^{-1} band was associated with Al—O and Si—O bonds. The 1651 cm^{-1} band corresponds to H—O—H bending, due to the presence of water molecules located within the zeolite channels and/or exchangeable cations [37]. The signal located at 2854 cm^{-1} and 2924 cm^{-1} corresponds to the presence of organic material occluded within the plerospheres and cenospheres of the material, which shows a compara-

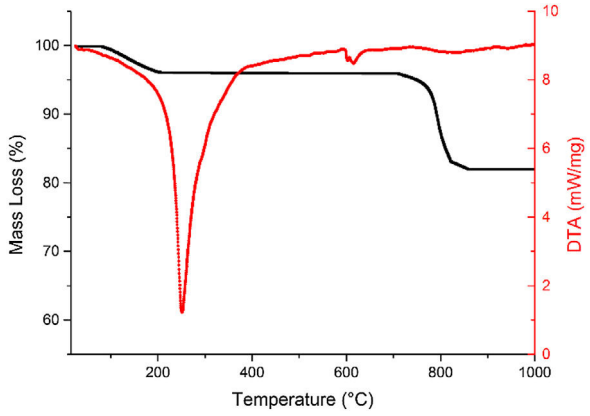

Fig. 13 – Thermal analysis of the synthesized Faujasite-Na zeolite performed between room temperature and 1000 °C.

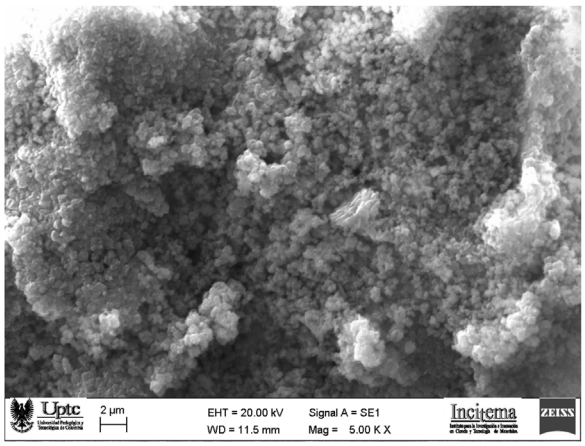

Fig. 15 – Scanning electron microscopy image of obtained Faujasite-Na.

ble reduction with the original FA, indicating that the thermal treatments had an effect on the removal of the unburned used as precursor material of the synthesized zeolite in agreement with Chen et al. [72]. The bands between 3450 and 3750 cm^{-1} are attributed to Si—OH type bonds and hydroxyl —OH groups as characteristically identified [71].

The thermal analysis of FAU material are shown in Fig. 13, where is evident a significant mass loss than in the case of FA, showing reductions of up to 17.2% with respect to the initial mass amount. The most important signal in the differential analysis is located above 251.3 °C and 1.1 mW mg^{-1}, corresponding to a mass loss of about 3.0%. This loss is expressed by the elimination of water molecules associated with the zeolite which may be condensed or polymerized by the presence of Si—OH and Al—OH bonds in the material. The second signal located above 602.0 °C corresponds to the presence of aluminosilicates, which extends from 580 °C to 610 °C and 8.3 mW mg^{-1} attributed to the formation of zeolite (Faujasite) and which is confirmed by contrasting the present results with those obtained by Chavez et al. [73] and Murukutti et al. [74].

The Faujasite-Na phase is stabilized above 700 °C with final mass losses of 17.2% and from which no further changes are shown in the synthesized material. The composition of the synthesized zeolite is observed in the energy dispersive X-ray fluorescence spectra shown in Fig. 14. The synthesized zeolite contains Na at 10.48% which agrees with the Faujasite-Na phase identified by XRD, and C, O, Al, Si and Ca at 1.16, 48.86, 14.64, 23.78 and 1.08% respectively. Sivalingam et al. [30] reported oxygen, aluminum, and silicon percentage values of 50.08, 21.88 and 25.35% in zeolite. On the other hand, Iqbal et al. [9] reports values of 15.9% for silicon, 19.6% for aluminum, and 15% for sodium.

Fig. 15 shows the micrograph of the FAU, where the change in morphology with respect to the FA or starting material was observed. The characteristic spheres of the FA changed from smooth surface to irregular, hexagonal and spherical shapes as corroborated by Abdelrahman et al. [59]. Particle size distribution is uniform with regular shape according to Reinoso et al. [28] and Mohammed et al. [23]. This change in morphology observed between the FA and the FAU is explained by a process of dissolution of the amorphous phase of the aluminosilicates present in the FA, followed by a process of nucleation and crystallization of zeotypes on the external surface of the spherical FA particles, developing pseudomorphs, considering that the resulting aggregates maintain the original shape of the spherical FA particles. However, Faujasite developed aggregates of crystals, which could indicate its

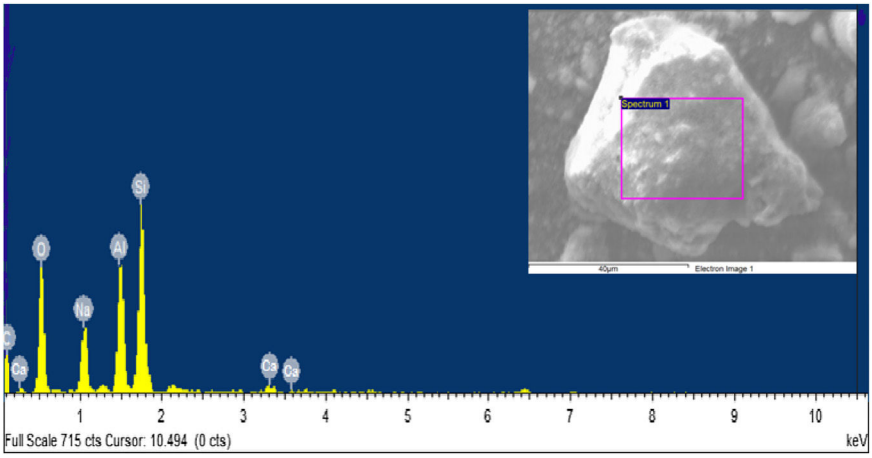

Fig. 14 – X-ray energy dispersive analysis of the synthesized FAU zeolite sample.

Table 6 – XRF patterns of the fly ash and Faujasite.

Component	Al	Si	K	Ca	Ti	Fe	Na
Fly ash (%)	23.90	54.10	3.07	0.74	2.57	15.60	–
Faujasite (%)	31.10	50.30	1.40	0.91	2.64	11.20	2.43

nucleation and growth outward from the surface of the spherical FA particles [75].

After melting with NaOH and hydrothermal treatment, spheres and agglomerates of fly ash become crystal structures with relatively complete morphology and much smaller particle size, as show in Fig. 7. In the case of the Faujasite synthesis, the crystallites of these phases are quite irregular and partially build up on the remains of unreacted aluminosilicates glass, forming separate crystals of some regularity [41]. Complementary to the X-ray diffraction results, the SEM images confirm the crystals formation of a FAU-type zeolite as has been reported by Koohsaryan et al. [76].

In agreement with previous results, the usefulness of FA as a precursor in the synthesis of FAU type zeolite is indicated. The characterization of the FA by XRD indicated the presence of mullite, quartz, sillimanite and lime, whose structure agrees with the Al—O—Al and Si—O—Si vibrations identified by FTIR, likewise the study of the elemental composition of the ash by EDX evidenced the presence of Si, Al, O and Ca; relevant elements in the identified structures.

The SEM studies allowed visualizing the spherical morphology characteristics corresponding to the glassy phases of aluminosilicates obtained by hydrothermal melting treatments. The morphology studied by SEM indicated the presence of irregular and hexagonal shapes characteristic of Faujasite-Na. The XRD the new structure formed was identified together with the presence of mullite and quartz remnants in minor quantities, meanwhile the FTIR, bands were attributed to internal tetrahedron deformations characteristic of zeolite, vibrations associated with double rings and D6R secondary structures, Si—O—Si bonds and H—O—H bending related to water located inside the zeolite were identified. The thermal analysis of FAU confirm the presence of aluminosilicates and the main signals attributed to the formation of Faujasite as main obtained material.

Table 6 shows the XRF results for the major components and in accordance with ASTM C618 standard, the FA could be classified as F class [37]. Such characteristics are relevant for identification of higher silicon concentrations in fly ashes due to relevance of SiO_2 associated to the presence of quartz phase and mullite in fly ash and aluminosilicates in Faujasite according to Feng et al. [2] and Akin et al. [18] Similarly Liu et al. [77] not reported presence of high sodium concentrations in these samples of Faujasite.

Fig. 16a shows the N_2 adsorption/desorption isotherms and pore size distribution curves of fly ash. The results confirm an uptake of N_2 increases steeply above the relative pressure of 0.95 for fly ash, showing a IV typical isotherm that is indicative of a mesoporous structure. The presence of the hysteresis loop at relative pressure ranging from 0.45 to 0.95 corresponding to type H3 of IUPAC classification, means that the particles are plate-like and have slit-like pores, these behavior is similar to reported by Ni et al. [78] in the sample of fly ash. Is clear

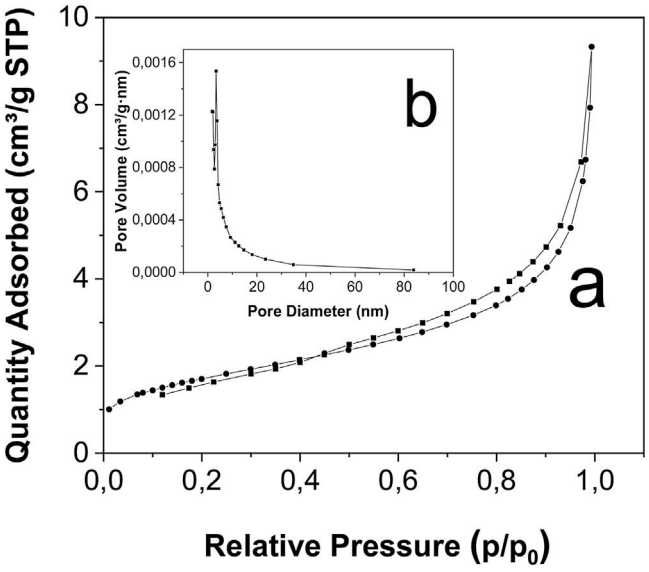

Fig. 16 – Nitrogen adsorption–desorption isotherms of FA and its pore volume distributions.

that the relative pressure of separation between adsorption curve and desorption curve exceeded the 0.4 value ($P/P_0 > 0.4$, where P is the adsorbent pressure and P_0 is the vapor pressure), indicating that this composite correspond to a mesoporous material [79]. The graph show the absence of an inflection point demonstrates the absence of micropores in the fly ash [58], this is related with a low surface area of the fly ash $6\,m^2\,g^{-1}$, these and others textural properties are listed in Table 7 in accordance with previous works in which the surface area for fly ash was $1.4\,m^2\,g^{-1}$ [80]; 1.5–$2.9\,m^2\,g^{-1}$ [51]; $2.6\,m^2\,g^{-1}$ [27] and $1.2\,m^2\,g^{-1}$ [48].

The corresponding BJH adsorption method (Barrett, Joyner and Halenda, Fig. 16b), show that the average pore size of the fly ash was 9.23 nm; this value is similar to the works of Li et al. [79], with pore sizes of 8.1 nm and average pore volumes of 0.01 ($cm^3\,g^{-1}$) for the fly ash in similar reaction conditions, validating the proposed synthesis method.

Fig. 17a shows the N_2 adsorption/desorption isotherms and pore size distribution curves of Faujasite. The behavior of Fig. 17 is characteristic of the Faujasite reported by Mohammed et al. [23]; Abdelrahman et al. [59]; Arroyave et al. [81] and El-kordy et al. [82], showing the hysteresis loop under the relative pressure of $(P/P_0) > 0.4$, which is a typical IV type isotherm with H3 hysteresis loop, indicating that the Faujasite has a typical mesoporous structure. Similar results were reported by Koohsaryan et al. [83]; He et al. [48]; Joseph et al. [37] and Laabd et al. [84] for the displayed Faujasite with hysteresis loops at relative pressures $(P/P_0) = 0.45$, which are associated with mesoporous networks and IV type isotherms according to the IUPAC.

Table 7 – Physical parameters of fly ash and faujasite.

Sample	S_{BET} (m^2/g)	Micropore volume (t-plot) ($cm^3\ g^{-1}$)	Pore volume ($cm^3\ g^{-1}$)	Pore size (nm)
Fly ash	6	0.00	0.01	9.23
Faujasite	460	0.18	0.16	8.15

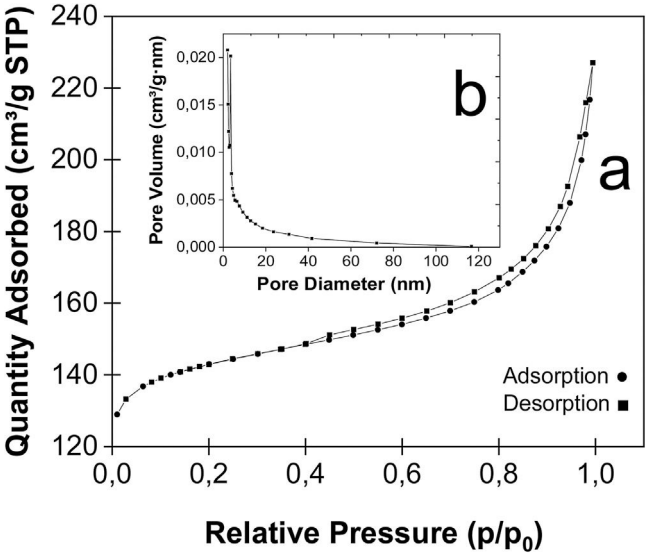

Fig. 17 – Nitrogen adsorption–desorption isotherms of Faujasite-Na and its pore volume distributions.

The above indicates that the formation of a monolayer of N_2 produce the coverage over the mesoporous walls of the material at $P/P_0 \geq 0.45$ values. The coverage (capillary condensation and pore filling) inside of the mesopores is consistent with other works [84], suggesting some mesoporous presence [28] with cylindrical characteristics [23,28,58]. These hysteresis at relative pressure between 0.45 and 0.85 is associated with slit-shaped pores [28], and the existence of intercrystalline pores between the Faujasite crystals [85]. El-kordy et al. [82] shows that synthetized Faujasite obtained isotherms are consistent with a IV type with a type H3 hysteresis according to the IUPAC classification, corroborating that these solids are mesoporous and similar to showed in Fig. 17b.

For the case of Faujasite, in Table 7 shows the surface area of 460 $m^2\ g^{-1}$, and although in other works the obtained values were 896 $m^2\ g^{-1}$ (Kuterasinski et al. [85]; 558.7 $m^2\ g^{-1}$; El-kordy et al. [82] 412 $m^2\ g^{-1}$; Gjyli et al. [51] and Mohammed et al. [23]) these differences, are attributed to the fact that in the first case, the porosity of Faujasite was hierarchical. Also, is evident that the hydrothermal temperature slightly affects the external surface area and pore volume. These results correspondence with higher smaller crystal size. An increase in the external surface area is consistent with a reduction in particle size due to the number of crystals per crystallites present in the material according to Reinoso et al. [28].

Table 7 shows that the obtained micropore volume of the Faujasite was 0.18 ($cm^3\ g^{-1}$), while in the works development by Joseph et al. [37] and Reinoso et al. [28], the Faujasite have a volume of 0.30 ($cm^3\ g^{-1}$) and report a micropore volume of 0.27 ($cm^3\ g^{-1}$) which confirm the effectiveness of proposed synthesis method. The specific surface area of fly ash was 6 $m^2\ g^{-1}$, while the specific surface area of synthetic zeolite increases to 460 $m^2\ g^{-1}$ after hydrothermal synthesis, which indicates that after the synthesis of zeolite, the specific surface area is greatly increased in almost 76 times.

The specific surface of the Faujasite is very large compared to that of the fly ash, this is due to the structural ordering, which yields very narrow pore size leading to optimal surface area, with the corresponding improve of the adsorption [48]. With respect to the obtained pore diameter of the Faujasite, it was 8.1 nm, while for Li et al. [86], is report a diameter of 4.7 nm, for Abdelrahman et al. [56] is reported pores diameter in the range of 2–50 nm and for Koohsaryan et al. [83] values around 2–10 nm. These parameters are important with regards to the sorption efficiency since it provide different channel sizes for transport of organic compounds, metals, and gases, thus allowing or blocking the possibility of adsorption [50], being an important feature of the Faujasite, which plays decisive role in determining its applications as catalyst, adsorbents and ion exchangers [86].

Conclusions

The proposed fusion-hydrothermal method allowed the efficient synthesis of Faujasite-Na (FAU) zeolites from fly ash (FA), which was demonstrated by the structural characterization of the starting material and the product obtained after the synthesis, where the presence of Faujasite-Na was evidenced by means of phase identification with X-ray diffraction and quantified using the Rietveld method where 62.28% of the zeolite was calculated in the synthesized material.

By means FTIR spectroscopy, the bands present in both materials were identified, observing the presence of similar vibrations for the aluminosilicates existing in the fly ash and the tetrahedral formed in the structure of the synthesized zeolite.

Elemental analysis by EDX allowed identifying the high percentages of oxygen, aluminum, and silicon present in the fly ash; main components for the synthesis of zeolites, additionally, lower percentages of calcium were identified, an element in lower proportion in the structure of the Faujasite-Na type zeolite. Scanning electron microscopy confirmed spherical shapes in the fly ash and crystal form in the Faujasite-Na, demonstrating the morphological transformation of the fly ash into another material after being subjected to the fusion-hydrothermal treatment in alkaline medium.

The TGA and DTA analysis evidence loss mass according with humidity elimination mainly associated with the zeolite phase and the presence of Si—OH and Al—OH bonds in the material in accordance with previous works.

BET studies conducted on the zeolite indicated that the material had a specific surface area of 460 $m^2\ g^{-1}$ and pore size of 8.1 nm demonstrating the effectiveness of proposed method to obtention of Faujasite-Na zeolites starting from fly ashes in

the context of providing solutions for the incorporation of fly ash in the dynamics of a circular economy.

REFERENCES

[1] L. Yang, X. Qian, P. Yuan, H. Bai, T. Mij, Green synthesis of zeolite 4A using fly ash fused with synergism of NaOH and Na_2CO_3, J. Clean. Prod. 212 (2019) 250–260, http://dx.doi.org/10.1016/j.jclepro.2018.11.259.

[2] W. Feng, Z. Wang, J. Daniels, Z. Li, Synthesis of high-quality zeolites from coal fly ash: mobility of hazardous elements and environmental applications, J. Clean. Prod. 202 (2018), http://dx.doi.org/10.1016/j.jclepro.2018.08.140.

[3] Z. Tauanov, D. Shah, V. Inglezakis, P.K. Jamwal, Hydrothermal synthesis of zeolite production from coal fly ash: a heuristic approach and its optimization for system identification of conversion, J. Clean. Prod. 182 (2018) 616–623, http://dx.doi.org/10.1016/j.jclepro.2018.02.047.

[4] G.L. Golewski, Energy savings associated with the use of fly ash and nanoadditives in the cement composition, Energies (Basel) 13 (2020), http://dx.doi.org/10.3390/en13092184.

[5] J.S. Mankar, S.S. Rayalu, R. Balasubramanian, R.J. Krupadam, High performance CO_2 capture at elevated temperatures by using cenospheres prepared from solid waste, fly ash, Chemosphere 284 (2021), http://dx.doi.org/10.1016/j.chemosphere.2021.131405.

[6] Y. Xing, F. Guo, M. Xu, X. Gui, H. Li, G. Li, Y. Xia, H. Hang, Separation of unburned carbon from coal fly ash: a review, Powder Technol. 353 (2019), http://dx.doi.org/10.1016/j.powtec.2019.05.037.

[7] A. Danish, M.A. Mosaberpanah, Formation mechanism and applications of cenospheres: a review, J. Mater. Sci. 55 (2020) 4539–4557, http://dx.doi.org/10.1007/s10853-019-04341-7.

[8] T. Hu, W. Gao, X. Liu, Y. Zhang, C. Meng, Synthesis of zeolites Na-A and Na-X from tablet compressed and calcinated coal fly ash, R. Soc. Open Sci. 4 (2017), http://dx.doi.org/10.1098/rsos.170921.

[9] A. Iqbal, H. Sattar, R. Haider, S. Munir, Synthesis and characterization of pure phase zeolite 4A from coal fly ash, J. Clean. Prod. 219 (2019), http://dx.doi.org/10.1016/j.jclepro.2019.02.066.

[10] M.G. Lee, J.W. Park, S.K. Kam, C.H. Lee, Synthesis of Na-A zeolite from Jeju Island scoria using fusion/hydrothermal method, Chemosphere 207 (2018) 203–208, http://dx.doi.org/10.1016/j.chemosphere.2018.05.080.

[11] Y.R. Lee, J.T. Soe, S. Zhang, J.W. Ahn, M.B. Park, W.S. Ahn, Synthesis of nanoporous materials via recycling coal fly ash and other solid wastes: a mini review, Chem. Eng. J. 317 (2017) 821–843, http://dx.doi.org/10.1016/j.cej.2017.02.124.

[12] G.I. Supelano, et al., Synthesis of magnetic zeolites from recycled fly ash for adsorption of methylene blue, Fuel 263 (2019), http://dx.doi.org/10.1016/j.fuel.2019.116800.

[13] J. Szerement, A. Szatanik-Kloc, R. Jarosz, T. Bajda, M. Mierzwa-Hersztek, Contemporary applications of natural and synthetic zeolites from fly ash in agriculture and environmental protection, J. Clean. Prod. 311 (2021), http://dx.doi.org/10.1016/j.jclepro.2021.127461.

[14] T. Ju, Y. Meng, S. Han, L. Lin, J. Jiang, On the state of the art of crystalline structure reconstruction of coal fly ash: a focus on zeolites, Chemosphere 283 (2021), http://dx.doi.org/10.1016/j.chemosphere.2021.131010.

[15] C. Liu, Y. Wang, J. Xia, L. Zhou, W. Zhang, Z. Zhang, Synthesis optimization and characterization of a novel zeolite produced from coal fly ash by hydrothermal reaction in alkaline solution, Energy Sources A: Recov. Util. Environ. Effects (2021) 1–12, http://dx.doi.org/10.1080/15567036.2021.1910385.

[16] W. Wulandari, T. Paramitha, J. Rizkiana, D. Sasongko, Characterization of zeolite A from coal fly ash via fusion-hydrothermal synthesis method, IOP Conf. Ser. Mater. Sci. Eng. 543 (2019), http://dx.doi.org/10.1088/1757-899X/543/1/012034.

[17] F. Collins, A. Rozhkovskaya, J.G. Outram, G.J. Millar, A critical review of waste resources, synthesis, and applications for Zeolite LTA, Micropor. Mesopor. Mater. 291 (2020), http://dx.doi.org/10.1016/j.micromeso.2019.109667.

[18] S.Ş. Akın, S.K. Kirdeciler, F. Kazanç, B. Akata, Critical analysis of zeolite 4A synthesis through one-pot fusion hydrothermal treatment approach for class F fly ash, Micropor. Mesopor. Mater. 325 (2021), http://dx.doi.org/10.1016/j.micromeso.2021.111338.

[19] M. Yoldi, E.G. Fuentes-Ordoñez, S.A. Korili, A. Gil, Zeolite synthesis from industrial wastes, Micropor. Mesopor. Mater. 287 (2019) 183–191, http://dx.doi.org/10.1016/j.micromeso.2019.06.009.

[20] X. Deng, P. Zhou, X. Yan, R. Xiong, H. Kou, W. Luo, Green synthesis of low-silica CHA zeolite without organic structural directing agents, fluoride media and seeds, Micropor. Mesopor. Mater. 310 (2021), http://dx.doi.org/10.1016/j.micromeso.2020.110618.

[21] X. Ren, S. Liu, R. Qu, L. Xiao, P. Hu, H. Song, W. Wu, C. Zheng, X. Wu, X. Gao, Synthesis and characterization of single-phase submicron zeolite Y from coal fly ash and its potential application for acetone adsorption, Micropor. Mesopor. Mater. 295 (2020), http://dx.doi.org/10.1016/j.micromeso.2019.109940.

[22] Y. Jin, L. Li, Z. Liu, S. Zhu, D. Wang, Synthesis and characterization of low-cost zeolite NaA from coal gangue by hydrothermal method, Adv. Powder Technol. 32 (2021) 791–801, http://dx.doi.org/10.1016/j.apt.2021.01.024.

[23] B. Mohammed, K. Yamni, N. Tijani, A. Alrashdi, H. Zouihri, Y. Dehmani, I. Chung, S. Kim, H. Lgaz, Adsorptive removal of phenol using faujasite-type Y zeolite: adsorption isotherms, kinetics and grand canonical Monte Carlo simulation studies, J. Mol. Liq. 296 (2019), http://dx.doi.org/10.1016/j.molliq.2019.111997.

[24] Z. Liu, C. Shi, D. Wu, S. He, B. Ren, A simple method of preparation of high silica zeolite y and its performance in the catalytic cracking of cumene, J. Nanotechnol. 2016 (2016), http://dx.doi.org/10.1155/2016/1486107.

[25] B. Reiprich, T. Weissenberger, W. Schwieger, A. Inayat, Layer-like FAU-type zeolites: a comparative view on different preparation routes, Front. Chem. Sci. Eng. 14 (2020) 127–142, http://dx.doi.org/10.1007/s11705-019-1883-3.

[26] T.A. Aragaw, A.A. Ayalew, Removal of water hardness using zeolite synthesized from Ethiopian kaolin by hydrothermal method, Water Pract. Technol. 14 (2019) 145–159, http://dx.doi.org/10.2166/wpt.2018.116.

[27] X. Ren, L. Xiao, R. Qu, S. Liu, D. Ye, H. Song, W. Wu, C. Zheng, X. Wu, X. Gao, Synthesis and characterization of a single-phase zeolite A using coal fly ash, RSC Adv. 8 (2018) 42200–42209, http://dx.doi.org/10.1039/c8ra09215j.

[28] D. Reinoso, M. Adrover, M. Pedernera, Green synthesis of nanocrystalline faujasite zeolite, Ultrason. Sonochem. 42 (2018) 303–309, http://dx.doi.org/10.1016/j.ultsonch.2017.11.034.

[29] Y. Liu, G. Wang, L. Wang, X. Li, Q. Luo, P. Na, Zeolite P synthesis based on fly ash and its removal of Cu(II) and Ni(II) ions, Chin. J. Chem. Eng. 27 (2019) 341–348, http://dx.doi.org/10.1016/j.cjche.2018.03.032.

[30] S. Sivalingam, S. Sen, Optimization of synthesis parameters and characterization of coal fly ash derived microporous zeolite X, Appl. Surf. Sci. 455 (2018) 903–910, http://dx.doi.org/10.1016/j.apsusc.2018.05.222.

[31] Y. Zhang, Y. Chen, W. Kang, H. Hang, H. Song, C. Zhang, H. Wang, X. Yang, X. Gong, C. Zhai, J. Deng, L. Ai, Excellent adsorption of Zn (II) using NaP zeolite adsorbent synthesized from coal fly ash via stage treatment, J. Clean. Prod. 258 (2020), http://dx.doi.org/10.1016/j.jclepro.2020.120736.
[32] Y. He, S. Tang, S. Yin, S. Li, Research progress on green synthesis of various high-purity zeolites from natural material-kaolin, J. Clean. Prod. 306 (2021), http://dx.doi.org/10.1016/j.jclepro.2021.127248.
[33] Z. Tauanov, S. Azat, A. Baibatyrova, A mini-review on coal fly ash properties, utilization and synthesis of zeolites, Int. J. Coal Prep. Util. (2020) 1–23, http://dx.doi.org/10.1080/19392699.2020.1788545.
[34] A. Khaleque, M. Alam, M. Hoque, S. Mondal, J. Haider, B. Xu, M. Johir, A. Karmakar, J. Zhou, M. Ahmed, M. Moni, Zeolite synthesis from low-cost materials and environmental applications: a review, Environ. Adv. 2 (2020), http://dx.doi.org/10.1016/j.envadv.2020.100019.
[35] S. Lin, X. Jiang, Y. Zhao, J. Yan, Zeolite greenly synthesized from fly ash and its resource utilization: a review, Sci. Total Environ. 851 (2022), http://dx.doi.org/10.1016/j.scitotenv.2022.158182.
[36] T. Paramitha, Conversion of Coal Fly Ash to Zeolite by Alkaline Fusion-Hydrothermal Method: A Review, 2020.
[37] I. Joseph, L. Tosheva, A.M. Doyle, Simultaneous removal of Cd (II), Co (II), Cu(II), Pb(II), and Zn(II) ions from aqueous solutions via adsorption on FAU-type zeolites prepared from coal fly ash, J. Environ. Chem. Eng. 8 (2020), http://dx.doi.org/10.1016/j.jece.2020.103895.
[38] K. Vegere, R. Kravcevica, A.E. Krauklis, T. Juhna, Comparative study of hydrothermal synthesis routes of zeolite A, Mater. Today Proc. 33 (2020) 1984–1987, http://dx.doi.org/10.1016/j.matpr.2020.06.326.
[39] Y. Zhang, L. Zhou, L. Chen, Y. Guo, F. Guo, J. Wu, B. Dai, Synthesis of zeolite Na-P1 from coal fly ash produced by gasification and its application as adsorbent for removal of Cr (VI) from water, Front. Chem. Sci. Eng. 15 (2021) 518–527, http://dx.doi.org/10.1007/s11705-020-1926-9.
[40] J.C. Arroyave-Manco, J.C. Arboleda-Echavarría, D.Á. Hoyos-Ayala, A.P. Echavarría-Isaza, LTA and FAU zeolites from coal combustion and residue by-products for chromium removal application, DYNA (Colombia) 85 (2018) 150–160, http://dx.doi.org/10.15446/dyna.v85n204.67096.
[41] P. Kunecki, R. Panek, M. Wdowin, T. Bień, W. Franus, Influence of the fly ash fraction after grinding process on the hydrothermal synthesis efficiency of Na-A, Na-P1, Na-X and sodalite zeolite types, Int. J. Coal Sci. Technol. 8 (2021), http://dx.doi.org/10.1007/s40789-020-00332-1.
[42] T. Degen, M. Sadki, E. Bron, U. König, G. Nénert, The high score suite, Powder Diffract. 29 (2014) 13–18, http://dx.doi.org/10.1017/S0885715614000840.
[43] B.H. Toby, R.B. von Dreele, GSAS-II: the genesis of a modern open-source all-purpose crystallography software package, J. Appl. Crystallogr. 46 (2013) 544–549, http://dx.doi.org/10.1107/S0021889813003531.
[44] S.R. Hall, F.H. Allen, I. David Brown, International Union of Crystallography Commission on Crystallographic Data Commission on Journals Working Party on Crystallographic Information The Crystallographic Information File (CIF): A New Standard Archive File for Crystallography, 1991.
[45] C.M. Clark, R.T. Downs, Using the American Mineralogist Crystal Structure Database in the classroom, J. Geosci. Educ. 52 (2004) 76–80, http://dx.doi.org/10.5408/1089-9995-52.1.76.
[46] X. Li, R. Snellings, K.L. Scrivener, Quantification of amorphous siliceous fly ash in hydrated blended cement pastes by X-ray powder diffraction, J. Appl. Crystallogr. 52 (2019) 1358–1370, http://dx.doi.org/10.1107/S1600576719013955.
[47] B. Amoni, A. Lima, R. Andrade, C. Pinto, Effect of coal fly ash treatments on synthesis of high-quality zeolite A as a potential additive for warm mix asphalt, Mater. Chem. Phys. 275 (2022), http://dx.doi.org/10.1016/j.matchemphys.2021.125197.
[48] X. He, B. Yao, Y. Xia, H. Huang, Y. Gan, W. Zhang, Coal fly ash derived zeolite for highly efficient removal of Ni^{2+} in waste water, Powder Technol. 367 (2020) 40–46, http://dx.doi.org/10.1016/j.powtec.2019.11.037.
[49] D. Längauer, V. Čablík, S. Hredzák, A. Zubrik, M. Matik, Z. Danková, Preparation of synthetic zeolites from coal fly ash by hydrothermal synthesis, Materials 14 (2021), http://dx.doi.org/10.3390/ma14051267.
[50] P. Nowak, B. Muir, A. Solinska, M. Franus, T. Bajda, Synthesis and characterization of zeolites produced from low-quality coal fly ash and wet flue gas desulphurization wastewater, Materials 14 (2021), http://dx.doi.org/10.3390/ma14061558.
[51] S. Gjyli, A. Korpa, V. Teneqja, D. Siliqi, C. Belviso, Siliceous Fly Ash Utilization Conditions for Zeolite Synthesis, vol. 6, 2021, http://dx.doi.org/10.3390/iecms2021-09359.
[52] R.J. Angel, C.T. Prewitt, Crystal structure of mullite: a re-examination of the average structure, Am. Mineral. 71 (1986) 1476–1482.
[53] J. Glinnemann, H.E. King Jr., H. Schulz, T. Hahn, S.J. La Placa, F. Dacol, Crystal structures of the low-temperature quartz-type phases of silica and germanium dioxide at elevated pressure, Z. Kristallogr. 198 (1992) 177–212.
[54] J.B. Burt, N.L. Ross, R.J. Angel, M. Koch, Equations of state and structures of andalusite to 9.8 GPa and sillimanite to 8.5 GPa, Am. Mineral. 91 (2006) 319–326, http://dx.doi.org/10.2138/am.2006.1875.
[55] P.E. Stutzman, L. Struble, Instructions in using GSAS Rietveld software for quantitative X-ray diffraction analysis of Portland clinker and cement, Gaithersburg (2015), http://dx.doi.org/10.6028/NIST.TN.1884.
[56] E. Abdelrahman, A. Alharbi, A. Subaihi, A. Hameed, M. Almutairi, F. Algethami, H. Youssef, Facile fabrication of novel analcime/sodium aluminum silicate hydrate and zeolite Y/faujasite mesoporous nanocomposites for efficient removal of Cu(II) and Pb(II) ions from aqueous media, J. Mater. Res. Technol. 9 (2020) 7900–7914, http://dx.doi.org/10.1016/j.jmrt.2020.05.052.
[57] S. Somderam, A.S. Abd Aziz, A.H. Abdullah, R. Mat, Characterisation of NAA zeolite made from Malaysian kaolin, Chem. Eng. Trans. 72 (2018) 325–330, http://dx.doi.org/10.3303/CET1972055.
[58] D. Novembre, D. Gimeno, A. Del Vecchio, Synthesis and characterization of Na-P1 (GIS) zeolite using a kaolinitic rock, Sci. Rep. 11 (2021) 1–11, http://dx.doi.org/10.1038/s41598-021-84383-7.
[59] E. Abdelrahman, A. Alharbi, A. Subaihi, A. Hameed, M. Almutairi, F. Algethami, H. Youssef, Facile fabrication of novel analcime/sodium aluminum silicate hydrate and zeolite Y/faujasite mesoporous nanocomposites for efficient removal of Cu (II) and Pb (II) ions from aqueous media, J. Mater. Res. Technol. 9 (2020) 7900–7914, http://dx.doi.org/10.1016/j.jmrt.2020.05.052.
[60] A. Hamadi, K. Nabih, Synthesis of zeolites materials using fly ash and oil shale ash and their applications in removing heavy metals from aqueous solutions, J. Chem. (2018), http://dx.doi.org/10.1155/2018/6207910.
[61] Y. Chen, S. Cong, Q. Wang, H. Hang, J. Lu, Y. Kang, W. Kang, H. Wang, H. Song, J. Zhang, Optimization of crystal growth of sub-micron ZSM-5 zeolite prepared by using $Al(OH)_3$ extracted from fly ash as an aluminum source, J. Hazard Mater. 349 (2018), http://dx.doi.org/10.1016/j.jhazmat.2018.01.004.

[62] A. Tironi, M.A. Trezza, E.F. Irassar, A.N. Scian, Thermal treatment of kaolin: effect on the pozzolanic activity, Proc. Mater. Sci. 1 (2012) 343–350, http://dx.doi.org/10.1016/j.mspro.2012.06.046.
[63] M. Valášková, Z. Klika, B. Novosad, B. Smetana, Crystallization and quantification of crystalline and non-crystalline phases in kaolin-based cordierites, Materials 12 (2019), http://dx.doi.org/10.3390/ma12193104.
[64] P.F. Prado, M. Nascimento, L. Yokoyama, O.G.C. Cunha, Use of coal ash in zeolite production and applications in manganese adsorption, AJER 12 (2017) 394–403.
[65] G. Ke, H. Shen, P. Yang, Synthesis of X-zeolite from waste basalt powder and its influencing factors and synthesis mechanism, Materials 12 (2019) 1–14, http://dx.doi.org/10.3390/ma122333895.
[66] S.K. Nayak, S.R. Mohanty, Zeolite Synthesis from Waste and its Applications: A Retrospective, 2019 [Online]. Available from: www.ijisrt.com.
[67] E. Strzałkowska, Z. Adamczyk, Influence of chemical composition of fly-ash cenospheres on their grains size, Int. J. Environ. Sci. Technol. 17 (2020) 809–818, http://dx.doi.org/10.1007/s13762-019-02512-2.
[68] Y. Zhang, Z. Leng, F. Zou, L. Wang, S.S. Chen, D.C.W. Tsang, Synthesis of zeolite A using sewage sludge ash for application in warm mix asphalt, J. Clean. Prod. 172 (2018) 686–695, http://dx.doi.org/10.1016/j.jclepro.2017.10.005.
[69] K. Momma, F. Izumi, VESTA 3 for three-dimensional visualization of crystal, volumetric and morphology data, J. Appl. Crystallogr. 44 (2011) 1272–1276, http://dx.doi.org/10.1107/S0021889811038970.
[70] E. Fernandez, Propiedades de los metales, Revista digital para profesionales de la enseñanza 16 (2011) 1–14.
[71] D. Nibou, S. Amokrane, H. Mekatel, N. Lebaili, Elaboration and characterization of solid materials of types zeolite NaA and faujasite NaY exchanged by zinc metallic ions Zn^{2+}, Phys. Proc. 2 (2009) 1433–1440, http://dx.doi.org/10.1016/j.phpro.2009.11.113.
[72] Y. Chen, S. Cong, Q. Wang, H. Hang, J. Lu, Y. Kang, W. Kang, H. Wang, H. Song, J. Zhang Optimization of crystal growth of sub-micron ZSM-5 zeolite prepared by using Al $(OH)_3$ extracted from fly ash as an aluminum source, J. Hazard. Mater. 349 (2018) 18–26, http://dx.doi.org/10.1016/j.jhazmat.2018.01.004.
[73] A. Chávez, G. Vargas, J.M. Almanza, Preparation and characterization of fly ash for use as ceramic coatings on metallic substrates, Boletin de la Sociedad Española de Cerámica y Vidrio 47 (2008) 333–338, http://dx.doi.org/10.3989/cyv.2008.v47.i6.158.
[74] M.K. Murukutti, H. Jena, Synthesis of nano-crystalline zeolite-A and zeolite-X from Indian coal fly ash, its characterization and performance evaluation for the removal of Cs^{+} and $Sr2^{+}$ from simulated nuclear waste, J. Hazard. Mater. (2022), http://dx.doi.org/10.1016/j.jhazmat.2021.127085.
[75] A. Lizcano, L. Cabeza, A. Ríos, L. Vargas, Efecto del proceso de fusión y envejecimiento en la síntesis de zeotipos a partir de cenizas volantes, Revista Facultad de Ingeniería Universidad de Antioquia 74 (2015) 213–225.
[76] P. Krongkrachang, P. Thungngern, P. Asawaworarit, HoungkaEiad-Ua, N. Apiluckmhang, Synthesis of Zeolite Y from Kaolin via hydrothermal method, Mater. Today Proc. 17 (2019) 1431–1436, http://dx.doi.org/10.1016/j.matpr.2019.06.164.
[77] Y. Liu, G. Wang, L. Wang, X. Li, Q. Luo, P. Na, Zeolite P synthesis based on fly ash and its removal of Cu (II) and Ni (II) ions, Chin. J. Chem. Eng. 27 (2019) 341–348, http://dx.doi.org/10.1016/j.cjche.2018.03.032.
[78] X. Ni, X. Sun, Y. Xu, D. Xu, A green and facile synthesis of nosean composite from coal fly ash for optimizing Rhodamine B adsorption using response surface methodology, J. Mol. Liq. 359 (2022), http://dx.doi.org/10.1016/j.molliq.2022.119262.
[79] G. Li, M. Li, X. Zhang, P. Cao, H. Jiang, J. Luo, T. Jiang, Hydrothermal synthesis of zeolites-calcium silicate hydrate composite from coal fly ash with co-activation of $Ca(OH)_2$-NaOH for aqueous heavy metals removal, Int. J. Min. Sci. Technol. 32 (2022) 563–573, http://dx.doi.org/10.1016/j.ijmst.2022.03.001.
[80] Y. Kobayashi, F. Ogata, T. Nakamura, N. Kawasaki, Synthesis of novel zeolites produced from fly ash by hydrothermal treatment in alkaline solution and its evaluation as an adsorbent for heavy metal removal, J. Environ. Chem. Eng. 8 (2020), http://dx.doi.org/10.1016/j.jece.2020.103687.
[81] J.C. Arroyave-manco, J.C. Arboleda, D.Á. Hoyos-ayala, A.P. Echavarría-isaza, LTA and FAU zeolites from coal combustion and residue by- products for Chromium removal application, Zeolitas LTA y FAU obtenidas a partir de cenizas volantes y su aplicación en remoción de Cromo 85 (2018) 150–160.
[82] A. -Kordy, A. Elgamouz, E. Lemdek, N. Tijani, S. Alharthi, A. Kawde, I. Shehadi, Preparation of sodalite and faujasite clay composite membranes and their utilization in the decontamination of dye effluents, Membranes (Basel) 12 (2022), http://dx.doi.org/10.3390/membranes12010012.
[83] E. Koohsaryan, M. Anbia, Facile and rapid synthesis of highly crystalline mesoporous zeolite FAU, Mater. Lett. 236 (2019) 390–393, http://dx.doi.org/10.1016/j.matlet.2018.10.139.
[84] M. Laabd, A. Imgharn, A. Hsini, Y. Naciri, M. Mobarak, S. Szunerits, R. Boukherrroub, A. Albourine, Efficient detoxification of Cr (VI)-containing effluents by sequential adsorption and reduction using a novel cysteine-doped PANi@faujasite composite: experimental study supported by advanced statistical physics prediction, J. Hazard Mater. 422 (2022), http://dx.doi.org/10.1016/j.jhazmat.2021.126857.
[85] U. Kuterasiński, M. Filek, B.D. Zimowska, M. Napruszewska, P.J. Gackowski, Jodłowski, Ultrasonically prepared mesoporous zeolites with faujasite type structure as catalysts for the production of diethyl ether and ethylene from ethanol, Mater. Res. Bull. 147 (2022), http://dx.doi.org/10.1016/j.materresbull.2021.111652.
[86] L. Li, Q. Shi, L. Huang, C. Yan, Y. Wu, Green synthesis of faujasite-$La_{0.6}Sr_{0.4}Co_{0.2}Fe_{0.8}O_3$-δ mineral nanocomposite membrane for low temperature advanced fuel cells, Int. J. Hydrogen Energy 46 (2021) 9826–9834, http://dx.doi.org/10.1016/j.ijhydene.2020.05.275.